

Title: Detecting Early Kidney Allograft Fibrosis with Multi-b-value Spectral Diffusion MRI

Authors: Mira M. Liu PhD¹, Jonathan Dyke PhD², Thomas Gladysz PhD³, Jonas Jasse BS⁴, Ian Bolger MS¹, Sergio Calle MS¹, Swathi Pavuluri BS¹, Tanner Crews BA², Surya Seshan MD⁵, Steven Salvatore MD⁵, Isaac Stillman MD⁶, Thangamani Muthukumar MD⁷, Bachir Taouli MD^{1,8}, Samira Farouk MD⁹, Octavia Bane PhD^{1,8,*}, and Sara Lewis MD^{1,8,*}

Author Affiliations:

¹BioMedical Engineering and Imaging Institute, Icahn School of Medicine at Mount Sinai, New York, NY, USA.

²Department of Radiology/Citigroup Biomedical Imaging Center, Weill Cornell Medicine, New York, NY, USA.

³Berlin Ultrahigh Field Facility (B.U.F.F.), Max Delbrück Center for Molecular Medicine in the Helmholtz Association, Berlin, Germany.

⁴Department of Diagnostic and Interventional Radiology, Medical Faculty and University Hospital Düsseldorf, Heinrich-Heine-University Düsseldorf, Düsseldorf, Germany

⁵Department of Pathology, Weill Cornell Medicine, New York, NY, USA.

⁶Department of Pathology, Icahn School of Medicine at Mount Sinai, Mount Sinai Hospital, New York, NY, USA.

⁷Department of Nephrology and Kidney Transplantation Medicine, Weill Cornell Medicine, New York, NY, USA

⁸Department of Diagnostic, Molecular and Interventional Radiology, Icahn School of Medicine at Mount Sinai, Mount Sinai Hospital, New York, NY, USA.

⁹Transplant Nephrology, Icahn School of Medicine at Mount Sinai, Mount Sinai Hospital, New York, NY, USA.

* O. Bane and S. Lewis are co-PI senior authors

*** Corresponding Author:**

Sara Lewis, MD

Professor of Diagnostic, Molecular and Interventional Radiology

BioMedical Engineering and Imaging Institute, Icahn School of Medicine at Mount Sinai

E-mail: Sara.Lewis@mountsinai.org

Acknowledgements

This project was funded by NIH NIDDK R01DK129888 (PI: Lewis/Bane) and supported by the National Center for Advancing Translational Sciences (NCATS) TL1TR004420 NRSA TL1 Training Core in Transdisciplinary Clinical and Translational Science (CTSA) (Fellow: Liu).

ABSTRACT

Kidney allograft fibrosis is a marker of chronic kidney disease (CKD) and predicts functional decline, and eventual allograft failure. This study evaluates if spectral diffusion MRI can help detect early development and mild/moderate fibrosis in kidney allografts. In a prospective two-center study of kidney allografts, interstitial fibrosis and tubular atrophy (IFTA) was scored and eGFR was calculated from serum creatinine. Multi-b-value DWI (bvalues = [0,10,30,50,80,120,200,400,800mm²/s]) was post-processed with spectral diffusion, intravoxel incoherent motion (IVIM), and apparent diffusion coefficient (ADC). Connection between imaging parameters and biological processes was measured by Mann-Whitney U-test and Spearman's rank; diagnostic ability was measured by five-fold cross-validation univariate and multi-variate logistic regression. Quality control analyses included volunteer MRI (n=4) and inter-observer analysis (n=19). 99 patients were included (50±13yo, 64M/35F, 39 IFTA=0, 22 IFTA=2, 20 IFTA=4, 18 IFTA=6, 46 eGFR≤45mL/min/1.73m², mean eGFR=47.5±21.3mL/min/1.73m²). Spectral diffusion detected fibrosis (IFTA > 0) in patients with normal/stable eGFR >

45ml/min/1.73m² [AUC(95%CI) = 0.72(0.56, 0.87), p = 0.007]. Spectral diffusion detected mild/moderate fibrosis (IFTA=2-4) [AUC(95%CI) = 0.65(0.52, 0.71), p = 0.023], as did ADC [AUC(95%CI) = 0.71(0.54, 0.87), p = 0.013]. eGFR, time-from-transplant, and allograft size could not. Interobserver correlation was ≥ 0.50 in 24/40 diffusion parameters. Spectral diffusion MRI showed detection of mild/moderate fibrosis and fibrosis before decline in function. It is a promising method to detect early development of fibrosis and CKD before progression.

Keywords: MRI, diffusion, kidney, kidney disease, allografts, fibrosis

Abbreviations and acronyms: intravoxel incoherent motion (IVIM), interstitial fibrosis and tubular atrophy (IFTA), estimated glomerular filtration rate (eGFR), area under the curve (AUC), confidence interval (CI)

INTRODUCTION

Kidney allograft interstitial fibrosis and tubular atrophy (IFTA) is a marker of chronic kidney disease (CKD)¹ and associated with allograft failure and increased patient mortality^{2,3}. While declining kidney function measured by an increase in serum creatinine in blood is a sign of CKD, the current reference standard of fibrosis is histopathology. This requires biopsy samples for diagnosis, staging of severity, continuous patient monitoring, as well as for studies of novel therapeutic outcome⁴. Further, fibrosis can develop silently before serum creatinine rises, and the time for intervention is lost as irreversible kidney damage occurs. As such, imaging may detect fibrosis without invasive biopsy, as well as provide information on kidney size, anatomy of the urinary system, and alternate diagnoses which biopsy and serum creatinine cannot. Noninvasive monitoring and subsequent early identification and quantification of fibrosis could enable therapeutic interventions that may preserve kidney function, including modifications in the patient's immunosuppressive regimen, and help screen for patients who may need further invasive biopsy.

Diffusion weighted magnetic resonance imaging (DWI) is a method of non-invasive measurement of kidney tissue diffusion characteristics without IV contrast, instead using diffusion weighting 'b-values'⁵⁻¹⁰. When a range of multiple b-values are used, the curve may diverge from a standard mono-exponential into a multi-exponential due to signal contribution from components with different diffusion coefficients. In the kidney, these components could include diffusion in the tissue parenchyma, kidney tubules, and capillary perfusion in vasculature. A such, multi-b-value DWI may add value to biopsy surveillance with whole kidney assessment of multiple physiologies to assess diagnosis, disease severity, and potential salvageability. Preliminary studies investigating multi-component model-free spectral diffusion in simulation¹¹⁻¹³, in healthy kidneys^{14,15}, and in native kidneys with CKD¹⁶ suggest kidney allografts with reduced function and fibrosis may benefit from spectral diffusion that is sensitive to different physiologic components within a voxel.

As a step towards clinical translation, we evaluate multi-b-value MRI for the noninvasive diagnosis and quantification of fibrosis and function in kidney allografts in a prospective two-center study. We compare multi-component spectral diffusion that allows one to three components (vascular perfusion, tubular flow, and tissue parenchyma)^{13,17} to two-component intravoxel incoherent motion (IVIM¹⁸; tissue component and vascular component^{7,19-23}), and standard

apparent diffusion coefficient (ADC). We then compare diagnostic ability of univariate and multiparametric logistic regression models built from these three diffusion models to those from standard clinical parameters to examine clinical relevance in early detection of fibrosis.

RESULTS

Patient Demographics and Clinical Characteristics

The demographics and clinical characteristics of all 99 patients (64M/35F, 50 ± 13 y) are included in Supplement A1. Comparisons between sites, and interobserver subset are included in Supplement A2. Four control-volunteers (1F/3M, 38.5 ± 11.8 y) were scanned at Site 1. Right native kidneys were chosen for analysis, to avoid tissue-air interface artifacts from the bowel, more prominent in the left kidney.

Diffusion Spectra

Example DWI ($b=0$), T2w HASTE and corresponding example voxels with multi-b-value DWI curves and corresponding diffusion spectra are shown in Figure 1. Diffusion model parameters (Table 1), as well as example spectral diffusion parameter maps (Figure 2) are included in methods and materials.

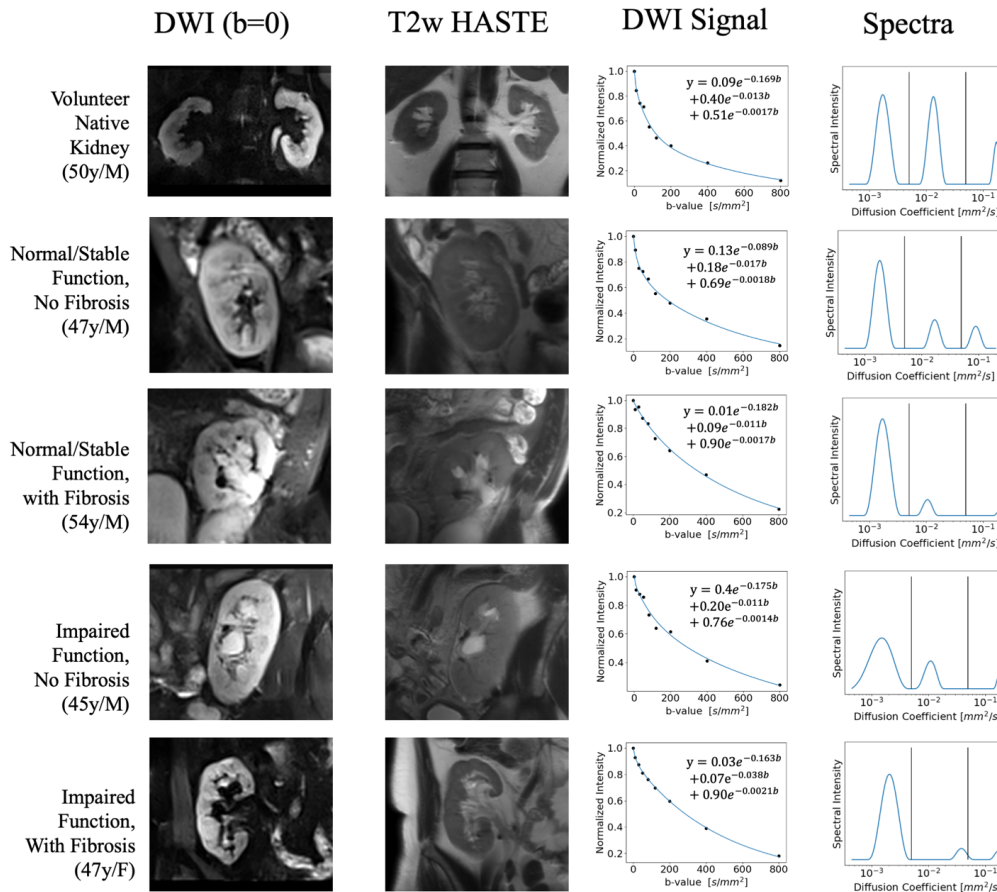


Figure 1. Example DWI and T2 weighted HASTE images of volunteer native kidneys and allografts for each of the four classifications of function and fibrosis, labeled for each row. An example multi-b value DWI curve from a voxel in each of the rows is shown in the third column. The corresponding diffusion spectrum is shown in the fourth column, with the multi-exponential fit resulting from the spectrum plotted on top of the DWI curve in the third

column. Vertical lines are shown to represent the boundaries used to separate spectral peaks (Supplement E).

Advanced Diffusion in Allografts Compared to Control Kidneys

The boxplot in Figure 3 shows fD_{tubule} decreasing between control kidneys, stable kidney allografts, and diseased allografts; in comparison, IVIM fD^* , and ADC showed no significant correlation.

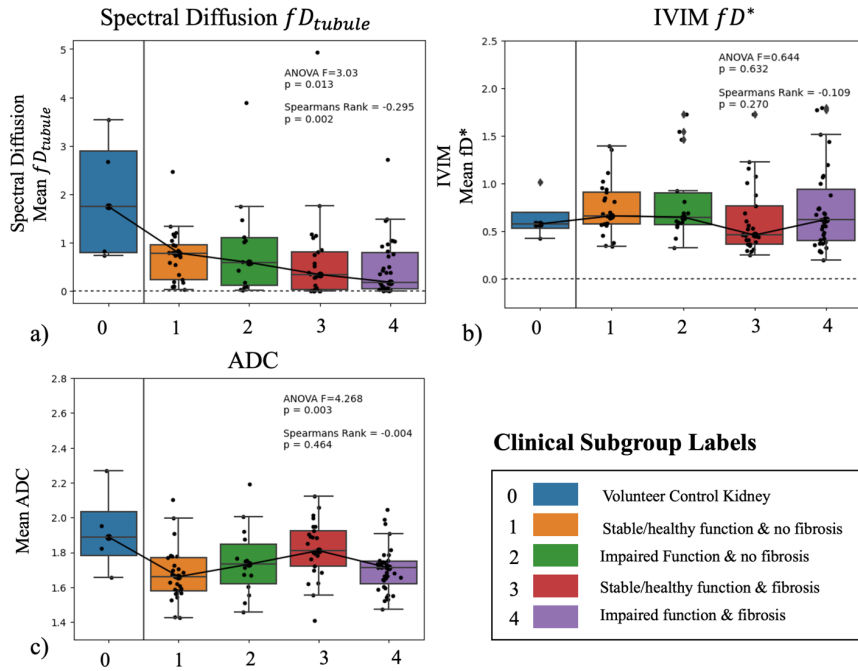


Figure 3. Box plots showing change in diffusion measured with a) spectral fD_{tubule} , b) IVIM fD^* , and c) ADC between volunteer native kidneys, and allografts with various renal functions and fibrosis scores. Kidneys were grouped ordinarily by degree of renal disease as control volunteers (0), healthy allografts (1) to allografts with both impaired function and fibrosis (4) shown in the legend. ‘Normal/stable function is determined as $eGFR > 45 \text{ ml/min/1.73m}^2$, and ‘fibrosis’ determined as $IFTA > 0$. A line connecting the mean values for each type of kidney is plotted to show the trend. As fraction f is unitless, and diffusion

coefficient D is in $10^{-3} \text{ mm}^2/\text{s}$ the units of fD and fD^* are $10^{-3} \text{ mm}^2/\text{s}$ and is a proxy for flow volume per unit time.

Detection of Fibrosis

Diffusion model parameters with both significant Mann-Whitney U-test and area-under-the-curves (AUCs) for fibrosis are provided in Table 2. Spectral diffusion detected fibrosis in allografts ($IFTA > 0$) with $AUC(95\%CI) = 0.69(0.59, 0.81)$, $p < 0.001$ (Table 2a). Allografts with fibrosis had significantly increased fD_{tissue} and fD_{tubule} , with reduced tubule and vascular component parameters. Mean fD_{tissue} [$AUC(95\%CI) = 0.66(0.55, 0.78)$, $p = 0.005$] returned the highest univariate AUC. IVIM std D was significant, but neither IVIM nor ADC multiparametric AUCs were significant.

Spectral diffusion detected mild/moderate fibrosis in allografts (interstitial fibrosis and tubular atrophy score ($IFTA$) = 0 vs. $IFTA = 1-4$; Table 2b), with $AUC(95\%CI) = 0.65(0.52, 0.77)$, $p = 0.02$. Allografts with mild/moderate fibrosis had increased tissue component parameters and reduced tubule and vascular component parameters. Mean fD_{tissue} [$AUC(95\%CI) = 0.67(0.55, 0.80)$, $p = 0.004$] again had the highest univariate AUC. While IVIM and ADC also returned significant features, IVIM and ADC multiparametric models were not significant.

Only spectral diffusion detected severe fibrosis (IFTA=0 vs. IFTA=5-6; Table 2c) with $AUC(95\%CI) = 0.68(0.52,0.85)$, $p = 0.026$. IVIM and ADC returned no significant features, and no significant multiparametric models. Results for every parameter across all fibrosis diagnoses are included in Supplement B.

Table 2. Diagnostic performance of MR parameters for (a) no fibrosis (IFTA=0) vs. fibrosis (IFTA >0), (b) no fibrosis vs. mild/moderate fibrosis (IFTA=1-4), and (c) no fibrosis vs. severe fibrosis (IFTA=5-6). Included are parameters with both Mann-Whitney U-test $p < 0.05$ and univariate logistic regression $p < 0.05$. Presented is the mean \pm stdev, Mann-Whitney U-test p-value, and five-fold cross-validation ROC analysis. Numbers of cases per category are shown in corresponding parentheses by each group. As f is unitless, and diffusion coefficient D is in $10^{-3} \text{ mm}^2/\text{s}$ the units of fD are $10^{-3} \text{ mm}^2/\text{s}$ and a proxy for flow volume per unit time.

Table 2a) Parameter	No Fibrosis (39) $\mu \pm \sigma$	Fibrosis (60) $\mu \pm \sigma$	p-val	AUC (95%CI)	SN	SP	J-stat cutoff
Spectral Diffusion							
mean fD_{tissue}	1.59 \pm 0.29	1.74 \pm 0.29	0.003	0.66(0.55, 0.78)	0.56	0.82	0.534
std f_{tissue}	0.18 \pm 0.04	0.15 \pm 0.06	0.004	0.66(0.55, 0.77)	0.64	0.65	0.500
std D_{tubule}	12.48 \pm 5.65	9.05 \pm 5.09	0.004	0.66(0.55, 0.76)	0.64	0.60	0.464
mean D_{tubule}	7.58 \pm 4.82	5.41 \pm 4.66	0.010	0.64(0.53, 0.75)	0.77	0.55	0.467
std D_{vasc}	85.05 \pm 8.62	70.11 \pm 26.88	0.011	0.64(0.54, 0.75)	0.85	0.52	0.468
mean f_{tubule}	0.09 \pm 0.06	0.07 \pm 0.05	0.012	0.63(0.51, 0.74)	0.46	0.78	0.503
median fD_{tissue}	1.52 \pm 0.29	1.67 \pm 0.29	0.013	0.64(0.52, 0.75)	0.67	0.62	0.495
std f_{tubule}	0.14 \pm 0.05	0.11 \pm 0.06	0.018	0.63(0.52, 0.75)	0.56	0.65	0.500
mean D_{vasc}	89.31 \pm 35.1	68.89 \pm 46.48	0.022	0.62(0.51, 0.73)	0.87	0.38	0.415
mean f_{tissue}	0.75 \pm 0.07	0.79 \pm 0.09	0.027	0.62(0.51, 0.73)	0.74	0.50	0.494
Multiparametric			<0.001	0.69(0.59, 0.81)	0.72	0.60	0.496
IVIM							
std D	0.25 \pm 0.07	0.21 \pm 0.06	0.009	0.64(0.53, 0.76)	0.44	0.80	0.507
Multiparametric			0.33	0.44(0.32, 0.56)	0.23	0.78	0.513
Table 2b) Parameter	No Fibrosis (39)	Mild/Moderate Fibrosis (40)	p-val	AUC (95%CI)	SN	SP	J-stat Cutoff
Spectral Diffusion							
mean fD_{tissue}	1.59 \pm 0.29	1.74 \pm 0.23	0.004	0.67(0.55, 0.80)	0.59	0.82	0.530
std D_{tubule}	12.48 \pm 5.65	9.18 \pm 5.2	0.008	0.65(0.53, 0.77)	0.74	0.55	0.431
median fD_{tissue}	1.52 \pm 0.29	1.67 \pm 0.26	0.013	0.65(0.53, 0.77)	0.74	0.55	0.431
mean f_{vasc}	0.07 \pm 0.03	0.05 \pm 0.04	0.020	0.63(0.51, 0.76)	0.72	0.68	0.499
Multiparametric			0.02	0.65(0.52, 0.77)	0.67	0.70	0.511
IVIM							
std D	0.25 \pm 0.07	0.21 \pm 0.06	0.007	0.66(0.54,0.78)	0.44	0.82	0.507
mean $(1 - f)D$	1.24 \pm 0.14	1.3 \pm 0.12	0.017	0.64(0.51, 0.76)	0.74	0.53	0.493
median $(1 - f)D$	1.26 \pm 0.14	1.32 \pm 0.12	0.025	0.63(0.51, 0.76)	0.69	0.55	0.496
Multiparametric			0.55	0.54(0.41, 0.67)	0.77	0.38	0.485
Table 2c)	No Fibrosis (39)	Severe Fibrosis (20)		AUC (95%CI)	SN	SP	J-stat Cutoff
Spectral Diffusion							
std f_{tissue}	0.18 \pm 0.04	0.14 \pm 0.03	0.002	0.74(0.61, 0.87)	0.54	0.90	0.501

std D_{vasc}	85.05±8.62	67.13±24.95	0.003	0.72(0.56, 0.89)	0.85	0.65	0.475
std f_{tubule}	0.14±0.05	0.11±0.04	0.028	0.66(0.51, 0.80)	0.54	0.75	0.501
Multiparametric			0.026	0.68(0.52, 0.85)	0.87	0.50	0.466

Detection of Fibrosis in Allografts with Normal/Stable Function

Diffusion model parameters with both significant Mann-Whitney U-test and AUCs for detecting fibrosis in allografts with normal/stable function are shown in Table 3. Spectral diffusion detected fibrosis in allografts presenting with normal/stable function [AUC(95%CI) = 0.72(0.56,0.87), $p < 0.01$] (Table 3a). Median fD_{tissue} [AUC(95%CI) = 0.70(0.55, 0.86), $p = 0.006$] had the highest univariate AUC for spectral diffusion. Both ADC and IVIM also showed an increase in the tissue component parameters in patients with fibrosis, but only ADC returned significant multi-parametric model (Table 3a).

Allografts with both impaired function and fibrosis showed increased tissue compartment heterogeneity and decreased tubule component parameters compared to healthy allografts (Table 3b). Spectral diffusion did not detect allografts with impaired function but no fibrosis; while stdev D_{tissue} was significant, it did not pass multiple comparisons correction. Results for every parameter across all clinical subgroups are included in Supplement C.

Table 3. Diagnostic performance of MR parameters between allografts with normal/stable function (eGFR>45ml/min/1.73m²) and no fibrosis (IFTA=0) versus (a) normal/stable function and fibrosis (IFTA>0), (b) impaired function and no fibrosis, and (c) impaired function (eGFR<45ml/min/1.73m²) and fibrosis. Included are parameters with both Mann-Whitney U-test $p < 0.05$ and univariate logistic regression $p < 0.05$. Presented are mean±stdev, Mann-Whitney U-test p-value, and five-fold cross validation ROC analysis. Numbers of cases per category are shown in corresponding parentheses by each group. As fraction f is unitless, and diffusion coefficient D is in 10⁻³ mm²/s the units of fD are 10⁻³ mm²/s and is a proxy for flow volume per unit time.

Table 3a)	Normal/stable function, no fibrosis (25)	Normal/stable function & fibrosis (25)	p-val	AUC(95%CI)	SN	SP	J-stat Cutoff
Spectral Diffusion							
median fD_{tissue}	1.51±0.26	1.74±0.31	0.006	0.70(0.55, 0.86)	0.76	0.68	0.469
median f_{tissue}	0.76±0.08	0.84±0.10	0.010	0.70(0.56, 0.85)	0.84	0.48	0.494
std D_{tubule}	11.8±3.92	8.69±5.37	0.018	0.67(0.51, 0.82)	0.76	0.56	0.433
std f_{vasc}	0.09±0.03	0.07±0.05	0.025	0.67(0.51, 0.83)	0.80	0.56	0.499
Multiparametric			0.007	0.72(0.56, 0.87)	0.84	0.64	0.464
IVIM							
std D	0.26± 0.06	0.2± 0.06	0.002	0.74(0.61, 0.88)	0.52	0.80	0.506
mean $(1 - f)D$	1.23± 0.15	1.33± 0.14	0.014	0.68(0.52, 0.84)	0.80	0.64	0.494
median $(1 - f)D$	1.25± 0.15	1.35± 0.13	0.013	0.69(0.54, 0.85)	0.72	0.64	0.499
Multiparametric			0.35	0.58(0.41, 0.75)	0.48	0.72	0.506
ADC							
mean ADC	1.68± 0.16	1.78± 0.18	0.025	0.69(0.54, 0.85)	0.64	0.80	0.510
median ADC	1.66± 0.15	1.79± 0.18	0.011	0.69(0.54, 0.85)	0.64	0.80	0.510

std ADC	0.33± 0.12	0.25± 0.08	0.017	0.67(0.51, 0.83)	0.52	0.80	0.516
Multiparametric			0.013	0.71(0.54, 0.87)	0.76	0.72	0.489
Table 3b)	Normal/stable function, no fibrosis (25)	Impaired function & fibrosis (35)	p-val	AUC(95%CI)	SN	SP	J-stat Cutoff
Spectral Diffusion							
std f_{tissue}	0.18±0.04	0.15±0.03	0.004	0.71(0.57, 0.85)	0.56	0.86	0.502
std D_{tissue}	1.0±0.28	0.90±0.69	0.006	0.69(0.55, 0.83)	0.76	0.54	0.490
mean f_{tubule}	0.10±0.06	0.06±0.05	0.016	0.65(0.51, 0.79)	0.52	0.74	0.501
std f_{tubule}	0.14±0.05	0.10±0.05	0.023	0.66(0.52, 0.80)	0.52	0.77	0.501
Multiparametric			0.021	0.67(0.52, 0.81)	0.68	0.63	0.491
IVIM							
std D	0.26± 0.06	0.22± 0.06	0.025	0.66(0.51, 0.80)	0.52	0.77	0.503
Multiparametric			0.29	0.58(0.43, 0.73)	0.56	0.63	0.500

Multi-Component fD Correlated with IFTA score

Spectral diffusion fD_{tissue} correlated positively with IFTA score in patients with normal/stable function (Spearman's rank = 0.359, $p < 0.01$; Figure 4a). fD_{tubule} correlated negatively with IFTA score (Figure 4b) while fD_{vasc} did not achieve statistical significance (Figure 4c). IVIM mean $(1 - f)D$ and mean ADC, both alternate measures of diffusion in tissue parenchyma, also correlated positively with IFTA score (Figure 4d-e).

Significant correlation was also seen between IFTA and fD across the entire patient cohort, i.e. not dichotomized by kidney function ($p = 0.005 - 0.045$). However, there was no significant correlation within the subset of patients presenting with impaired function ($p = 0.158 - 0.521$). Correlation was predominately in those presenting with normal/stable function.

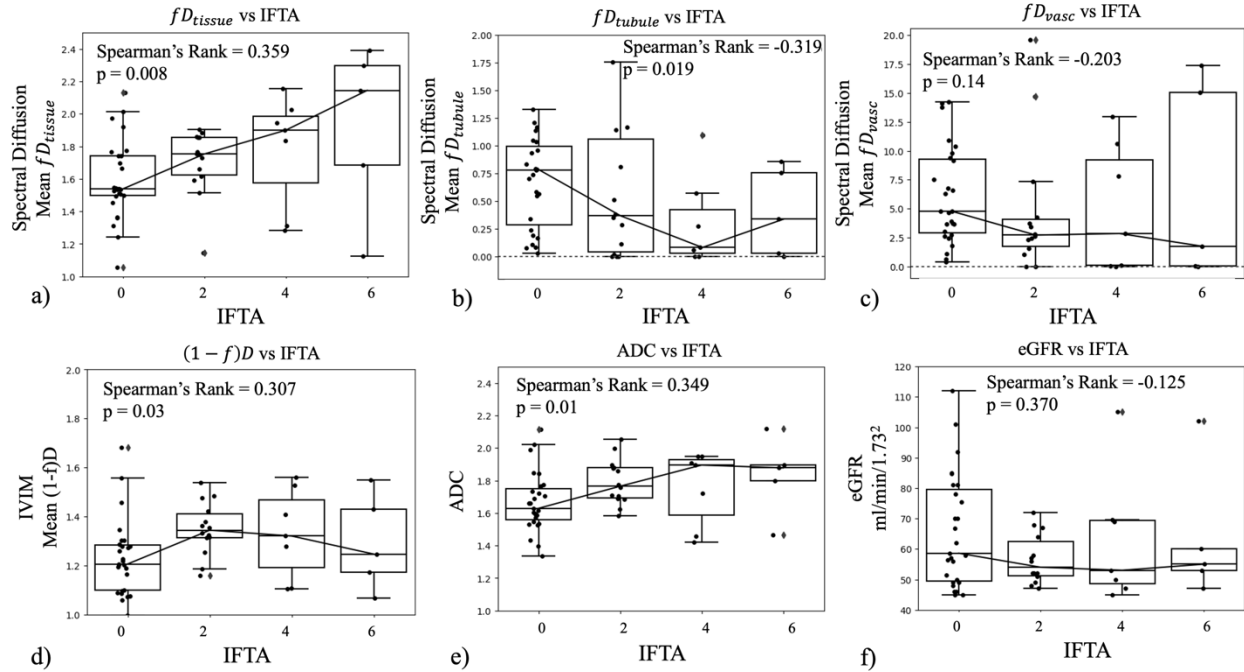


Figure 4. The top row shows spectral diffusion parameters of **a)** mean fD_{tissue} , **b)** mean fD_{tubule} , and **c)** mean fD_{vasc} correlated against Banff 2017 IFTA scores in patients presenting with normal/stable $eGFR > 45$ ml/min/1.73m². The bottom row shows the same correlations for **d)** IVIM mean $(1-f)D$, **e)** mean ADC, and **f)** CKD-EPI $eGFR$.

Diagnosis of Fibrosis with Clinical Parameters

Estimated glomerular filtration rate ($eGFR$) detected fibrosis with $AUC(95\%CI) = 0.63(0.52,0.74)$, $p = 0.027$ (IFTA=0 vs. IFTA>0; Table 4). However, $eGFR$ could not differentiate between no fibrosis and mild/moderate fibrosis or detect fibrosis if $eGFR > 45$ ml/min/1.73m². Further, $eGFR$ showed no correlation with fibrosis *within* the subsets of either normal/stable $eGFR$ (Spearman's rank = -0.125 , $p = 0.370$; Figure 4F) or impaired $eGFR$ (Spearman's rank = -0.128 , $p = 0.520$). Instead, $eGFR$ differentiated between the severe fibrosis and mild/moderate fibrosis (Table 4) and correlated with IFTA score across *all* patients (Spearman's rank = -0.342 , $p < 0.01$)

Allografts without fibrosis had shorter transplant intervals than those with severe fibrosis, i.e. an allograft was more likely to have developed fibrosis over time (Table 4). However, transplant interval was not significant for any other comparison in this study. Allograft volume, patient age, and BMI were not significant ($p > 0.10$) for any comparisons.

Table 4. Clinical demographic features $eGFR$, transplant-to-MRI interval (days), and allograft volume, for thresholding and grouping of IFTA. Included are parameters with both Mann-Whitney U-test $p < 0.05$ and univariate logistic regression $p < 0.05$. Presented is the mean \pm stdev, Mann-Whitney U-test p-value, and five-fold cross-validation ROC analysis. Numbers of cases per category are shown in corresponding parentheses by each group. No IFTA: ci+ct=0; mild/moderate IFTA: ci+ct= 1-4, severe IFTA: ci+ct= 5-6. Units of $eGFR$ are in 45ml/min/1.73m².

Table 4)	No Fibrosis (39)	Fibrosis (60)	p-val	AUC (95%CI)	SN	SP	J-stat Cutoff
$eGFR$	54.08 \pm 23.67	43.16 \pm 18.36	0.014	0.63(0.52, 0.74)	0.65	0.58	0.485

	No Fibrosis (39) $\mu \pm \sigma$	Severe Fibrosis (20) $\mu \pm \sigma$	p-val	AUC (95%CI)	SN	SP	J-stat Cutoff
eGFR	54.08±23.67	36.3±19.81	0.003	0.72(0.58, 0.86)	0.74	0.70	0.422
Transplant Interval	886±1679	2080±2454	0.015	0.71(0.55, 0.86)	0.85	0.50	0.495
	Mild/Moderate Fibrosis (40) $\mu \pm \sigma$	Severe Fibrosis (20) $\mu \pm \sigma$	p-val	AUC (95%CI)	SN	SP	J-stat Cutoff
eGFR	46.59±16.55	36.3±19.81	0.012	0.68(0.53, 0.83)	0.65	0.75	0.489
Transplant Interval	1107±1783	2082±2454	0.016	0.63(0.48, 0.78)	0.69	0.55	0.533

Combined MR Diffusion and eGFR

Combined spectral diffusion parameters and eGFR detected fibrosis (IFTA=0 vs IFTA>0), but it did not outperform spectral diffusion alone [AUC(95%) = 0.68(0.58, 0.79), $p < 0.01$; DeLong $p = 0.58$]. Spectral diffusion alone had the highest AUC for detection of mild/moderate IFTA. Inclusion of eGFR, allograft volume, Transplant-to-MRI interval, patient age, and patient BMI decreased the mean AUC, which is expected as they were not significant.

Interobserver Reproducibility and SNR

Interobserver correlation ranged from poor to excellent (ICC range=0.03-0.92) with 5/40 features returning an ICC between 0 and 0.25, 11/40 features returning an ICC between 0.25 and 0.50, 14/40 with an ICC between 0.50 and 0.75, and 10/40 with ICC above 0.75. Tissue diffusion components showed better interobserver reliability than tubular components, and IVIM and ADC demonstrated better ICC and CoV(%) than spectral diffusion. A full table of all ICC and CoV% is included in Supplement D. The signal-to-noise ratio of the DWI b=0 kidney allografts, after motion correction and denoising, ranged from 30 to 50.

DISCUSSION:

Spectral diffusion was able to detect fibrosis and demonstrated good sensitivity for mild/moderate fibrosis that IVIM, ADC, eGFR, time-from-transplant, and allograft size did not. Further, it detected fibrosis in allografts that were still presenting with normal/stable eGFR. This could enable early detection of CKD before a decline in kidney function is evident, and inform decisions to pursue biopsy or change the medication regimen, as well as longitudinal monitoring in clinical trials of anti-fibrotic medications²⁴⁻²⁶.

This study expanded spectral diffusion from simulation¹¹ and control volunteers^{14,15} to clinical translation of a multi-component diffusion model that includes more aspects of renal physiology. Unlike ADC²⁷, MR elastography²⁸, and IVIM²⁹, spectral diffusion separates diffusion components beyond vascular perfusion and tissue structure to provide insight into complex renal tubule physiology. Allografts showed lower tubular and tissue diffusion than volunteers, agreeing

with previously observed reduced diffusion and fluid transport³⁰. Allografts with fibrosis also had lower vascular and tubular parameters which supports detecting damaged microvasculature and tubules in fibrotic and dysfunctional kidneys³¹.

Across clinical comparisons, the tissue component showed the most clinical utility¹⁵. The fibrotic allografts had increased fD_{tissue} , supporting correlation with increased collagen deposition. While D_{tissue} might be expected to decrease with fibrosis due to greater diffusion restriction from collagen, the increase in signal fraction of f_{tissue} made the product fD_{tissue} increase with fibrosis. This suggests fD_{tissue} detects fibrous allograft tissue from the greater amount of the restricted diffusion, rather than slowed diffusion. Spectral diffusion improved diagnostic ability compared to IVIM D (using a bi-exponential to remove fast diffusion contamination) or ADC with $b > 200$ (excluding low b-values dominated by fast diffusion signal). This supports advanced separation of diffusion components in kidney disease³² to remove signal contamination from the tissue diffusion component and provide signal fraction.

Spectral diffusion separated mild/moderate fibrosis from no fibrosis while eGFR, allograft size, and time-to-transplant did not. Detection of mild/moderate fibrosis is clinically important as it may allow preventative intervention and treatment. Spectral diffusion could be another clinical measure, in addition to proteinuria, donor-derived cell-free DNA, and creatinine³³⁻³⁵ for fibrosis detection and assessment of progression. Further, eGFR only significantly decreased once there were high levels of fibrosis, agreeing with current clinical knowledge; decreased eGFR tends to be a marker post the stage of irreversible fibrosis and considerable scarring³⁶. In comparison, spectral diffusion detected fibrosis even when eGFR was normal/stable. This supports spectral diffusion detecting early change in microstructural diffusion patterns in the kidney and not being solely an indirect and more costly measure of GFR^{11,13,15}.

Results support fD as a parameter of interest for multi-component flow in the kidney¹³. fD of the vascular, tubule, and tissue components were significant and improved AUC values, as did IVIM $(1 - f)D$. fD_{tubule} correlating negatively against IFTA scores supports detection of renal filtrate and tubule destruction in patients presenting with normal/stable function. Similarly, the positive correlation of fD_{tissue} against IFTA scores supports detecting collagen deposition with nephron degeneration and tubular injury in allografts, rather lower ADC observed in native kidneys³⁷. As there have been mixed results regarding reduced ADC detecting restricted diffusion in allografts, these results support fD_{tissue} that includes the diffusion fraction may be a potential alternate along with previously observed corticomedullar difference^{7,38,39}.

Finally, spectral did not distinguish between fibrosis and no fibrosis for the subset with impaired function, nor between normal/stable function and impaired function for the subset with fibrosis. This highlights an important caveat: if a patient demonstrated impaired eGFR, spectral diffusion did not determine if the impaired allograft was fibrotic or not. However, detection of early fibrosis in patients presenting with normal/stable function remains clinically relevant.

We recognize several limitations. Further study is needed of spectral diffusion peak sorting, multi-component rigid models^{8,40}, and parameter stability. Whole cortex segmentation rather than circular ROIs may improve coverage and interobserver reliability, at the cost of artifacts. T2

effects, corticomedullary difference, and the influence of anisotropic collecting tubules in the medulla was beyond the scope of this work in allografts, but has shown promise in CKD of native kidneys¹⁶. Longitudinal study is needed to test if spectral diffusion can be an early predictor of fibrosis and function decline, and study of immune rejection in addition to fibrosis is warranted given that this is a potentially confounding pathologic variable⁷. While this study demonstrated potential clinical translation of fD , validation of fD as a flow proxy may benefit from comparison to phantoms, complex simulations, microspheres, and flow cytometry in animal models^{13,41}, and radiotracers in human studies. This study included both protocol biopsies and clinically indicated biopsies which have some patient bias in terms of selection.

This work supports multi-component spectral diffusion detecting mild/moderate fibrosis development prior to kidney function decline, and correlation with fibrosis severity. Spectral diffusion could allow early intervention and preventative modification in medication regimen and treatment and reduce the need for repeated invasive biopsy or suggesting biopsy for potential intervention in patients still demonstrating healthy function. It could also contribute to longitudinal and novel therapeutic studies of fibrosis and CKD in kidney allografts.

MATERIALS AND METHODS:

Patients

This is a prospective, IRB-approved HIPAA-compliant two-center study at the Icahn school of Medicine at Mount Sinai and Weill Cornell Medicine that consists of kidney transplant recipients referred for percutaneous clinically indicated biopsies due to impaired allograft function or normal/stable function undergoing percutaneous protocol biopsies due to the presence of donor specific antibodies. Patients included in the study were those enrolled from 2/2022-09/2024 who are >1-month post-transplant. Informed consent was obtained, and patients underwent a non-contrast MRI protocol within 7 days of biopsy that included advanced DWI, as well as arterial spin labeling (ASL), blood oxygen level dependent imaging (BOLD), $T_1\rho$, T_1 relaxometry, and anatomical sequences (T2 HASTE, T1 in/opposed phase) that are beyond the scope of this current study. Exclusion criteria were age <18 years, large vessel or urinary tract complication of the kidney transplant, contra-indications to MRI, or pre-existing medical conditions including a likelihood of developing seizures or claustrophobic reactions. All experiments were performed in accordance with the Declaration of Helsinki, and allografts were procured according to the standard of care for subjects enrolled in the study at the Icahn school of Medicine at Mount Sinai and at Weill Cornell Medicine following relevant guidelines and regulations.

Image Acquisition

Patients underwent identical MR protocol with a 3T MRI (Mount Sinai: Skyra, Siemens Healthcare, Cornell: Prisma, Siemens Healthcare), set up by the same investigator at both sites, with a 16-channel body array and 32-channel spine array coils. The advanced DWI protocol was 2D coronal spoiled gradient echo-planar IVIM-DWI from the Siemens Advanced Body Diffusion

works-in-progress package (WIP-990N) with respiratory gating (by liver-dome tracking, pencil-beam navigator). Averaged and motion-corrected trace-weighted DWIs were exported directly from the scanner with ‘motion-corrected (MOCO)-averages’, ‘MOCO b-values’, ‘MOCO-3D’, ‘rescale local bias corruption’ and denoising⁴² selected for all 9 b-values (b-values = [0, 10, 30, 50, 80, 120, 200, 400, 800 s/mm²]; TR/TE = 1500/58ms, voxel size = 2x2x5mm³, 4-directions, 16 slices, 3-averages, acquisition time ~7-15minutes). Control volunteers underwent the same protocol at Site 1.

Image Analysis

Six circular regions-of-interest (average ROI size: 64±25mm²) were delineated at the renal hilum on motion corrected b=0 s/mm² by a radiologist (Observer 1, 13 years of experience) using T₂-weighted images as reference (Horos v. 3.2.1, www.horosproject.org). Two ROIs were selected each at the upper pole, midpole, and lower pole, and propagated to each motion-corrected b-value. Voxel-wise analysis outperformed ROI-averaged signal and so is reported in this work.

Spectral Diffusion Post-Processing

The diffusion spectra of voxel-wise DWI decay curves within each ROI were calculated using non-negative least squares (NNLS) in MATLAB (Mathworks Inc, 2023b). The voxel-wise signal as a function of increasing b-value were fit to 300 logarithmically spaced D values (log₁₀(5)-log₁₀(2200)) as an unconstrained sum of exponentials (Eq. 1)^{13 11,43}.

$$y_i = \sum_{j=1}^M s_j e^{-b_i D_j} \quad (1)$$

In Eq. 1, y_i is the equation for each of the N=9 b-values, for M=300 D values. y_i as a function of b-value is the equation fit to the DWI decay curve. Minimizing the difference between Eq. 1 and the DWI decay curve, with Tikhonov regularization to smooth in the presence of noise, outputs a diffusion spectrum of the contributions of all 300 exponential basis vectors¹¹. λ was set at 0.1 to match optimal $\lambda \approx \frac{\#bval}{SNR}$ ¹¹ and reduce computation time.

$$\chi_r^2 = \min \left[\sum_{i=1}^N \left| \sum_j^M s_j e^{-b_i D_j} - y_i \right|^2 + \lambda \sum_{j=2}^{M-1} |s_{j+1} - 2s_j + s_{j-1}|^2 \right] \quad (2)$$

The resulting spectra have peaks that represent the dominant basis vectors (Figure 1) per voxel without a priori assumption of number of peaks. Each peak returns a signal fraction f and mean diffusion coefficient D , and spectral peaks can be sorted into (1) vascular, (2) tubular, and (3) tissue parenchyma components. A diffusion spectrum with three components would fit a tri-exponential equation as follows.

$$\frac{S_b}{S_{b0}} = f_{vasc} e^{-bD_{vasc}} + f_{tubule} e^{-bD_{tubule}} + f_{tissue} e^{-bD_{tissue}} \quad (3)$$

Voxels with $R^2 < 0.70$ were excluded from analysis. Example MR images with sample advanced DWI decay curve and spectral analysis are shown in Figure 1. Table 1 provides parameter definitions and the physiologic processes they may represent. Further detail regarding the fitting and analysis of diffusion spectra is included in Supplement E.

IVIM and ADC Post-processing

The voxel-wise DWI decay curve was fit to standard IVIM bi-exponential, $fe^{-bD^*} + (1-f)e^{-bD}$, with a Bayesian-log estimation⁴⁴ given priors $\log D$ mean = 6.2 ± 1 and $\log D^*$ mean = 3.5 ± 1 ⁴⁵. A mono-exponential apparent diffusion coefficient (ADC) was calculated with a least-squares linear log fit of the signal from $b = 200, 400, 800 \text{ s/mm}^2$. This excluded IVIM effects at low b-values and non-Gaussian effects at high b-values²⁶. Voxels with $R^2 < 0.70$ were excluded from analysis.

Multi-component Diffusion fD Parameter

A parameter fD was calculated for each diffusion component as the product of the fraction and diffusion coefficient of the individual spectral peaks as described by Liu et al¹³ (Supplement E). In standard bi-exponential IVIM, fD^* has been used as a marker of blood flow in a capillary network^{19,20,46-48}. In this study, fD was used as an estimate of local intravoxel ‘flow’ of every component¹³. fD_{vasc} estimated the vascular motion, fD_{tubule} estimated tubular motion, and fD_{tissue} estimated total tissue diffusion in volume/time. For the standard bi-exponential, IVIM fD^* and $(1-f)D$ were used to estimate the ‘flow’ of vascular and tissue components respectively. Figure 2 illustrates fD of the three components.

Table 1. Spectral DWI parameters with corresponding hypothesized physiologic interpretation in the kidney cortex. Within the kidney cortex there are glomeruli, convoluted tubules, collecting ducts, and blood vessels. Conventional IVIM parameters are f and D^* for f_{vasc} and D_{vasc} , and D for D_{tissue} ; there is no tubular component.

Compartment	Spectral Parameters	Physiologic interpretation
Vascular: Vasculature in the kidney cortex is composed of blood vessels including arteries, veins, and capillaries.	f_{vasc}	Fraction of a voxel that is within blood vessels
	D_{vasc}	Diffusion coefficient, or speed, of the blood travelling within the vessels (D^* in conventional IVIM)
	fD_{vasc}	Proxy for the total blood flow in the vasculature. (fD^* in conventional IVIM)
Tubular: Kidney tubules in the nephrons filter the glomerular filtrate and return nutrients to blood through reabsorption. The remaining fluid and waste become urine. In the cortex there are glomeruli and convoluted tubules.	f_{tubule}	Fraction of a voxel that is within these tubules (no parameters in conventional IVIM)
	D_{tubule}	Diffusion coefficient of the tubular filtrate (no parameters in conventional IVIM)

	fD_{tubule}	Proxy for the total tubular flow in the renal tubules (no parameters in conventional IVIM)
Tissue Parenchyma: The kidney contains solid tissue, vascular endothelial cells, and tubular epithelial cells. Diffusion in the tissue parenchyma includes passive diffusion across cell membranes, and within the extracellular matrix (ECM) of the kidney parenchyma. Fibrosis in the kidney is a pathological feature that occurs when there is an excessive ECM accumulation leading to scarring and renal dysfunction.	f_{tissue}	Fraction of a voxel that is composed of these solid cells in the kidney parenchyma with and without ECM accumulation. ($1 - f$ in IVIM,
	D_{tissue}	Diffusion coefficient of molecules within the parenchyma and composed of tissue both with and without ECM accumulation.
	fD_{tissue}	Proxy for the total restricted diffusive flow within solid tissue structure, cells, and in ECM scarring.

Interobserver Agreement

Circular ROIs (average ROI size: $78 \pm 14 \text{ mm}^2$) sampling the cortex of a subset of $n=19$ allografts, chosen from each clinical subgroup blinded to images, were delineated by an independent observer (Observer 2, a medical student with 1 year of experience) blind to original ROIs and diagnoses. Interobserver agreement was calculated via intraclass correlation coefficient (ICC) and coefficient of variation (CoV%) for all MR parameters. ROI placement and ROI size were not standardized between the two observers, but slice selection was held constant.

Kidney Volume Measurement

For assessment of three-dimensional volumetric measurement of the allograft in milliliters (ml), T1 in-phase images were copied to a post-processing workstation (Vitreia core, Vital Images, Minnetonka, MN, USA). Three-dimensional reconstruction was performed using semi-automated interposition based on signal intensity differences of the allograft compared to the surrounding tissues by Observer 1.

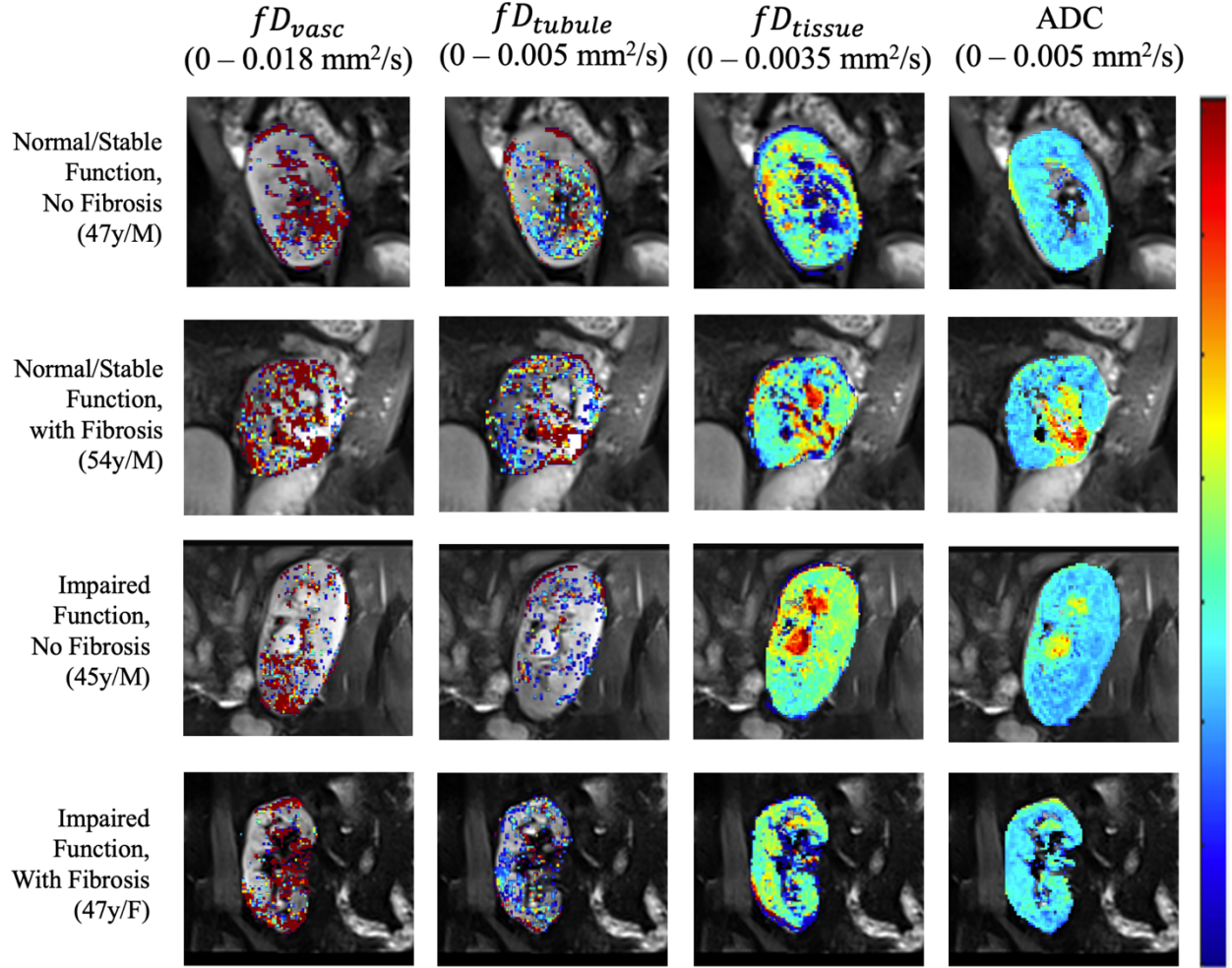


Figure 2. Images of different fD components and ADC, superimposed on each respective $b=0$ DWI from Figure 1. These images are solely for illustration; they were not used for measurement. Unlike IVIM and ADC, spectral diffusion allows a flexible number of compartments and compartments that return 0 are indistinguishable from noise. As such, vascular and tubular images appear noisy. The trend of decreased tubular and vascular flow in diseased allografts can be seen. Note the difference in scale for the three compartments with fD_{vasc} having the largest range, and fD_{tissue} having the smallest.

Laboratory Values and Histopathology

Serum creatinine was collected at time of imaging or biopsy for measurement of eGFR calculated with race agnostic CKD-EPI 2021 criteria⁴⁹. Interstitial fibrosis and tubular atrophy (IFTA=ci+ct) scores (range, 0-6) by pathologists were extracted from the clinical biopsy report, scored according to the Banff 2017 classification⁵⁰. Other Banff diagnoses within the allograft specimens were also recorded⁵⁰ (Supplement F), but inflammation/rejection is beyond the scope of this study.

Diagnostic Classifications and Clinical Subgroups

IFTA score was used to diagnose fibrosis (no fibrosis: IFTA=0, fibrosis: IFTA>0), and fibrosis severity (mild/moderate: IFTA=1-4, severe: IFTA=5-6). Normal/stable allograft function was determined as $eGFR \geq 45 \text{ ml/min/1.73m}^2$, and impaired function determined as $eGFR <$

45ml/min/1.73m². A threshold of 45ml/min/1.73m² was used to compensate for single kidney filtration. Allografts were further divided into clinical subgroups: allografts with (1) normal/stable function and no fibrosis, (2) impaired function no fibrosis, (3) normal/stable function and fibrosis, (4) impaired function and fibrosis.

Statistical Analysis and Machine Learning

To examine direct connection between imaging parameters and biological processes, histogram characteristics voxel-wise mean, median, and standard deviation of the cortical ROIs were analyzed with respect to laboratory values and diagnoses. Central tendency measures (mean, median) of each component's fD were included as MR parameters. Significant parameters were determined with Mann-Whitney U-test $p < 0.05$. The Benjamini-Hochberg procedure was applied for multiple comparisons corrections with a generous false discovery rate of 0.20, set to reduce false negatives in a novel method. Correlation of MR parameters against IFTA score was calculated with Spearman's rank and difference between clinical subgroups determined with ANOVA.

To examine diagnostic ability of imaging parameters and their direct relation to underlying physiology, univariate supervised machine learning logistic regression were built using significant histogram parameters with 5-fold cross validation. Diagnostic performance was assessed via receiver operating characteristic (ROC) and area-under-the-curve (AUC); mean AUC and 95% confidence interval (95%CI) was calculated via bootstrapping, and AUCs compared via the DeLong test. Sensitivity (SN), specificity (SP), and the optimal probability cutoff was calculated at the Youden's J-statistic (J-stat cutoff).

To compare overall diagnostic ability, one multiparametric model was built using parameters from each sequence (spectral diffusion, IVIM, and ADC) with 5-fold cross-validation for each diagnostic classification. Histogram characteristics for the multiparametric models were chosen as parameters that had $p < 0.05$ within training sets. This reduced data leakage and model overfitting in a small preliminary dataset. All statistical analysis and machine learning was performed in Python 3.11.4 (Anaconda Inc., 2024).

Code Availability

The code developed for spectral diffusion analysis in this work is available at https://github.com/miramliu/Spectral_Diffusion

Bibliography

1. Romagnani P, Remuzzi G, Glasscock R, Levin A, Jager KJ, Tonelli M, et al. Chronic kidney disease. *Nature Reviews Disease Primers*. 2017;3(1).
2. Mannon RB, Matas AJ, Grande J, Leduc R, Connett J, Kasiske B, et al. Inflammation in Areas of Tubular Atrophy in Kidney Allograft Biopsies: A Potent Predictor of Allograft Failure. *American Journal of Transplantation*. 2010;10(9).
3. Mengel M. Deconstructing interstitial fibrosis and tubular atrophy: a step toward precision medicine in renal transplantation. *Kidney International*. 2017;92(3).
4. Ho QY, Lim CC, Tan HZ, Sultana R, Kee T, Htay H. Complications of Percutaneous Kidney Allograft Biopsy: Systematic Review and Meta-analysis. *Transplantation*. 2022;106(7).
5. Leung G, Kirpalani A, Szeto SG, Deeb M, Foltz W, Simmons CA, et al. Could MRI Be Used To Image Kidney Fibrosis? A Review of Recent Advances and Remaining Barriers. *Clinical Journal of the American Society of Nephrology*. 2017;12(6).
6. Elsinger MM, Viteri B, Otero HJ, Bhatti T, Morales T, Roberts TPL, et al. Imaging fibrosis in pediatric kidney transplantation: A pilot study. *Pediatric Transplantation*. 2023;27(5).
7. Bane O, Hectors SJ, Gordic S, Kennedy P, Wagner M, Weiss A, et al. Multiparametric magnetic resonance imaging shows promising results to assess renal transplant dysfunction with fibrosis. *Kidney International*. 2020;97(2).
8. van Baalen S, Leemans A, Dik P, Lilien MR, ten Haken B, Froeling M. Intravoxel incoherent motion modeling in the kidneys: Comparison of mono-, bi-, and triexponential fit. *Journal of Magnetic Resonance Imaging*. 2017;46(1).
9. van der Bel R, Gurney-Champion OJ, Froeling M, Stroes ESG, Nederveen AJ, Krediet CTP. A tri-exponential model for intravoxel incoherent motion analysis of the human kidney: In silico and during pharmacological renal perfusion modulation. *European Journal of Radiology*. 2017;91.
10. Fan M, Xing Z, Du Y, Pan L, Sun Y, He X. Quantitative assessment of renal allograft pathologic changes: comparisons of mono-exponential and bi-exponential models using diffusion-weighted imaging. *Quantitative Imaging in Medicine and Surgery*. 2020;10(6).
11. Periquito JS, Gladysz T, Millward JM, Delgado PR, Cantow K, Grosenick D, et al. Continuous diffusion spectrum computation for diffusion-weighted magnetic resonance imaging of the kidney tubule system. *Quantitative Imaging in Medicine and Surgery*. 2021;11(7).
12. Jasse J, Wittsack H-J, Thiel TA, Zukovs R, Valentin B, Antoch G, et al. Toward Optimal Fitting Parameters for Multi-Exponential DWI Image Analysis of the Human Kidney: A Simulation Study Comparing Different Fitting Algorithms. *Mathematics*. 2024;12(4).
13. Liu M, Gladysz T, Dyke J, Bolger I, Jasse J, Calle S, et al. Estimation of Multi-Component Flow in the Kidney with Multi-b-value Spectral Diffusion. *Magn Reson Imaging*. 2025.
14. Stabinska J, Wittsack HJ, Lerman LO, Ljimini A, Sigmund EE. Probing Renal Microstructure and Function with Advanced Diffusion MRI: Concepts, Applications, Challenges, and Future Directions. *Journal of Magnetic Resonance Imaging*. 2023.
15. Stabinska J, Ljimini A, Zöllner HJ, Wilken E, Benkert T, Limberg J, et al. Spectral diffusion analysis of kidney intravoxel incoherent motion MRI in healthy volunteers and patients with renal pathologies. *Magnetic Resonance in Medicine*. 2021;85(6).
16. Hu W, Dai Y, Liu F, Yang T, Wang Y, Shen Y, et al. Assessing renal interstitial fibrosis using compartmental, non-compartmental, and model-free diffusion MRI approaches. *Insights into Imaging*. 2024;15(1).

17. Wurnig MC, Germann M, Boss A. Is there evidence for more than two diffusion components in abdominal organs? – A magnetic resonance imaging study in healthy volunteers. *NMR in Biomedicine*. 2017;31(1).
18. Le Bihan D, Breton E, Lallemand D, Aubin ML, Vignaud J, Laval-Jeantet M. Separation of diffusion and perfusion in intravoxel incoherent motion MR imaging. *Radiology*. 1988;168(2).
19. Le Bihan D. What can we see with IVIM MRI? *NeuroImage*. 2019;187.
20. Federau C, O'Brien K, Meuli R, Hagmann P, Maeder P. Measuring brain perfusion with intravoxel incoherent motion (IVIM): Initial clinical experience. *Journal of Magnetic Resonance Imaging*. 2013;39(3).
21. Wang W, Yu Y, Chen J, Zhang L, Li X. Intravoxel incoherent motion diffusion-weighted imaging for predicting kidney allograft function decline: comparison with clinical parameters. *Insights into Imaging*. 2024;15(1).
22. Hectors SJ, Lewis S, Kennedy P, Bane O, Said D, Segall M, et al. Assessment of Hepatocellular Carcinoma Response to 90Y Radioembolization Using Dynamic Contrast Material-enhanced MRI and Intravoxel Incoherent Motion Diffusion-weighted Imaging. *Radiology: Imaging Cancer*. 2020;2(4).
23. Zhang M-C, Li X-H, Huang S-Y, Mao R, Fang Z-N, Cao Q-H, et al. IVIM with fractional perfusion as a novel biomarker for detecting and grading intestinal fibrosis in Crohn's disease. *European Radiology*. 2018;29(6).
24. Thoeny HC, Grenier N. Science to Practice: Can Diffusion-weighted MR Imaging Findings Be Used as Biomarkers to Monitor the Progression of Renal Fibrosis? *Radiology*. 2010;255(3).
25. Rankin AJ, Mayne K, Allwood-Spiers S, Hall Barrientos P, Roditi G, Gillis KA, et al. Will advances in functional renal magnetic resonance imaging translate to the nephrology clinic? *Nephrology*. 2021;27(3).
26. Ljimini A, Caroli A, Laustsen C, Francis S, Mendichovszky IA, Bane O, et al. Consensus-based technical recommendations for clinical translation of renal diffusion-weighted MRI. *Magnetic Resonance Materials in Physics, Biology and Medicine*. 2019;33(1).
27. Zhang JL, Sigmund EE, Chandarana H, Rusinek H, Chen Q, Vivier P-H, et al. Variability of Renal Apparent Diffusion Coefficients: Limitations of the Monoexponential Model for Diffusion Quantification. *Radiology*. 2010;254(3).
28. Lee CU, Glockner JF, Glaser KJ, Yin M, Chen J, Kawashima A, et al. MR Elastography in Renal Transplant Patients and Correlation with Renal Allograft Biopsy. *Academic Radiology*. 2012;19(7).
29. Mao W, Zhou J, Zeng M, Ding Y, Qu L, Chen C, et al. Intravoxel incoherent motion diffusion-weighted imaging for the assessment of renal fibrosis of chronic kidney disease: A preliminary study. *Magnetic Resonance Imaging*. 2018;47.
30. Eisenberger U, Thoeny HC, Binser T, Gugger M, Frey FJ, Boesch C, et al. Evaluation of renal allograft function early after transplantation with diffusion-weighted MR imaging. *European Radiology*. 2009;20(6).
31. Kaissling B, LeHir M, Kriz W. Renal epithelial injury and fibrosis. *Biochimica et Biophysica Acta (BBA) - Molecular Basis of Disease*. 2013;1832(7).
32. Bane O, Seeliger E, Cox E, Stabinska J, Bechler E, Lewis S, et al. Renal MRI: From Nephron to NMR Signal. *Journal of Magnetic Resonance Imaging*. 2023;58(6).
33. Ponticelli C, Graziani G. Proteinuria after kidney transplantation. *Transplant International*. 2012;25(9).

34. Leotta C, Hernandez L, Tothova L, Arefin S, Ciceri P, Cozzolino MG, et al. Levels of Cell-Free DNA in Kidney Failure Patients before and after Renal Transplantation. *Cells*. 2023;12(24).
35. Bu L, Gupta G, Pai A, Anand S, Stites E, Moinuddin I, et al. Clinical outcomes from the Assessing Donor-derived cell-free DNA Monitoring Insights of kidney Allografts with Longitudinal surveillance (ADMIRAL) study. *Kidney International*. 2022;101(4).
36. Boor P, Floege J. Renal Allograft Fibrosis: Biology and Therapeutic Targets. *American Journal of Transplantation*. 2015;15(4).
37. Ferguson CM, Eirin A, Abumoawad A, Saad A, Jiang K, Hedayat AF, et al. Renal fibrosis detected by diffusion-weighted magnetic resonance imaging remains unchanged despite treatment in subjects with renovascular disease. *Scientific Reports*. 2020;10(1).
38. Beck-Tölly A, Eder M, Beitzke D, Eskandary F, Agibetov A, Lampichler K, et al. Magnetic Resonance Imaging for Evaluation of Interstitial Fibrosis in Kidney Allografts. *Transplantation Direct*. 2020;6(8).
39. Berchtold L, Crowe LA, Combescure C, Kassai M, Aslam I, Legouis D, et al. Diffusion-magnetic resonance imaging predicts decline of kidney function in chronic kidney disease and in patients with a kidney allograft. *Kidney International*. 2022;101(4).
40. Jiang K, Ferguson CM, Lerman LO. Noninvasive assessment of renal fibrosis by magnetic resonance imaging and ultrasound techniques. *Translational Research*. 2019;209.
41. Hammond TG, Majewski R. Analysis and isolation of renal tubular cells by flow cytometry. *Kidney International*. 1992;42(4).
42. Kannengiesser S, Mailhe B, Nada M, Huber S, Kiefer B. Universal iterative denoising of complex-valued volumetric MR image data using supplementary information. *Proc Intl Soc Mag Reson Med 24 (2016)*. 2016.
43. Bjarnason TA, Mitchell JR. AnalyzeNNLS: Magnetic resonance multiexponential decay image analysis. *Journal of Magnetic Resonance*. 2010;206(2).
44. Neil JJ, Bretthorst GL. On the use of bayesian probability theory for analysis of exponential decay date: An example taken from intravoxel incoherent motion experiments. *Magnetic Resonance in Medicine*. 2005;29(5).
45. Jerome NP, Orton MR, d'Arcy JA, Collins DJ, Koh DM, Leach MO. Comparison of free-breathing with navigator-controlled acquisition regimes in abdominal diffusion-weighted magnetic resonance images: Effect on ADC and IVIM statistics. *Journal of Magnetic Resonance Imaging*. 2013;39(1).
46. Federau C. Intravoxel incoherent motion MRI as a means to measure in vivo perfusion: A review of the evidence. *NMR in Biomedicine*. 2017;30(11).
47. Liu M, Saadat N, Roth S, Niekrasz M, Giurcanu M, Carroll T, et al. Quantification of Collateral Supply with Local-AIF Dynamic Susceptibility Contrast MRI Predicts Infarct Growth. *AJNR American journal of neuroradiology*. 2024;46(1).
48. Liu M, Saadat N, Jeong Y, Roth S, Niekrasz M, Giurcanu M, et al. Quantitative perfusion and water transport time model from multi b-value diffusion magnetic resonance imaging validated against neutron capture microspheres. *Journal of Medical Imaging*. 2023;10(06).
49. Delgado C, Baweja M, Crews DC, Eneanya ND, Gadegbeku CA, Inker LA, et al. A Unifying Approach for GFR Estimation: Recommendations of the NKF-ASN Task Force on Reassessing the Inclusion of Race in Diagnosing Kidney Disease. *American Journal of Kidney Diseases*. 2022;79(2).
50. Haas M, Loupy A, Lefaucheur C, Roufosse C, Glotz D, Seron D, et al. The Banff 2017 Kidney Meeting Report: Revised diagnostic criteria for chronic active T cell-mediated rejection,

antibody-mediated rejection, and prospects for integrative endpoints for next-generation clinical trials. *American Journal of Transplantation*. 2018;18(2).

51. Federau C, Wintermark M, Christensen S, Mlynash M, Marcellus DG, Zhu G, et al. Collateral blood flow measurement with intravoxel incoherent motion perfusion imaging in hyperacute brain stroke. *Neurology*. 2019;92(21).

52. Liu MM, Saadat N, Roth SP, Niekrasz MA, Giurcanu M, Shazeeb MS, et al. A Method for Imaging the Ischemic Penumbra with MRI using IVIM. *American Journal of Neuroradiology*. 2025.

53. Calamante F, Gadian DG, Connelly A. Delay and dispersion effects in dynamic susceptibility contrast MRI: Simulations using singular value decomposition. *Magnetic Resonance in Medicine*. 2000;44(3).

54. Liu MM, Saadat N, Roth SP, Niekrasz MA, Giurcanu M, Carroll TJ, et al. Quantification of Collateral Supply with Local-AIF Dynamic Susceptibility Contrast MRI Predicts Infarct Growth. *American Journal of Neuroradiology*. 2024.

55. Iutaka T, de Freitas MB, Omar SS, Scortegagna FA, Nael K, Nunes RH, et al. Arterial Spin Labeling: Techniques, Clinical Applications, and Interpretation. *RadioGraphics*. 2023;43(1).

56. Kim DW, Shim WH, Yoon SK, Oh JY, Kim JK, Jung H, et al. Measurement of arterial transit time and renal blood flow using pseudocontinuous ASL MRI with multiple post-labeling delays: Feasibility, reproducibility, and variation. *Journal of Magnetic Resonance Imaging*. 2017;46(3).

57. Cutajar M, Mendichovszky IA, Tofts PS, Gordon I. The importance of AIF ROI selection in DCE-MRI renography: Reproducibility and variability of renal perfusion and filtration. *European Journal of Radiology*. 2010;74(3).

58. Mouannes-Srour JJ, Shin W, Ansari SA, Hurley MC, Vakil P, Bendok BR, et al. Correction for arterial-tissue delay and dispersion in absolute quantitative cerebral perfusion DSC MR imaging. *Magn Reson Med*. Aug 2012;68(2).

Supplement A1. Patient demographics.

Demographics and Clinical Features	
Site	71 Site 1, 28 Site 2
Biopsy Type	
Indication Biopsy	N=71
Protocol Biopsy	N=28
Sex(F/M)	35/64
Race	
Black/African American	46
White	20
Asian	8
Other/Unreported	25
Age (years; mean \pm std, range)	50.1 \pm 13.1 (22-82)
Weight (kg; mean \pm std, range)	79.1 \pm 16.9 (44.5-129.0)
BMI (kg/m ² , mean \pm std, range)	27.4 \pm 4.7 (17.4-38.2)
Allograft Volume (mL, mean \pm std, range)	238 \pm 72 (100-573)
Living Donor	N=43;
Donor Age (years; mean \pm std, range)	44.6 \pm 12.0 (21-68)
Deceased Donor	N=54;
Donor Age (years; mean \pm std, range)	37.25 \pm 12.6 (5-70)*
KDPI	All KDPI < 85
Time since transplant (months; mean \pm std, range)	42.9 \pm 61.9 (1.3-266)
U-Protein (mg/24hr; mean \pm std, range)	140.6 \pm 257.8 (1.0-1513), 39 unknown
Calcium Inhibitor status	89 Tacrolimus, 4 Cyclosporine, 6 none
Donor Specific Antibodies status	80 negative, 12 positive, 7 unknown
eGFR (CKD-EPI 2021 mL/min/1.73m²; mean\pmstd, range)	47.5 \pm 21.3 (8.0-112.0)
eGFR \leq 45 (mL/min/1.73m ² ; mean \pm std, range)	N=46; 29.9 \pm 8.4 (8.0-44.0)
eGFR> 45 (mL/min/1.73m ² ; mean \pm std, range)	N=53; 62.7 \pm 16.9 (45.0-112.0)
Interstitial Fibrosis/ Tubular Atrophy (IFTA)	
IFTA = 0	39
IFTA = 2	22
IFTA = 4	20
IFTA = 6	18
Categories	
eGFR>45 & IFTA=0	25
eGFR>45 & IFTA>0	25
eGFR \leq 45 & IFTA=0	14
eGFR \leq 45 & IFTA>0	35

*one pediatric donor

Supplement A2. Demographic features for the subset of 19 cases used in interobserver comparison.

Demographics and Clinical Features	
Site	14 Site 1, 5 Site 2
Biopsy Type	
Indication Biopsy	N=14
Protocol Biopsy	N=5
Sex(F/M)	8/11
Age (years; mean±std, range)	48.7±12.9 (25-69)
BMI (kg/m ² , mean±std, range)	28.3±4.5 (20.7-38.2)
Living Donor	N=10;
Deceased Donor	N=9; All KDPI < 85
Time since transplant (months; mean±std, range)	53.2±62.7 (2.0-205)
U-Protein (mg/24hr; mean±std, range)	140.6±257.8 (1.0-1513), 39 unknown
Calcium Inhibitor status	18 Tacrolimus, 0 Cyclosporine, 1 none
Donor Specific Antibodies status	17 negative, 1 positive, 1 unknown
eGFR (CKD-EPI 2021 mL/min/1.73m²; mean±std, range)	40.2±18.0 (14.0-85.0)
eGFR ≤ 45 (mL/min/1.73m ² ; mean±std, range)	N=12; 29.4±10.4 (14.0-42.0)
eGFR > 45 (mL/min/1.73m ² ; mean±std, range)	N=7; 58.5±12.7 (45.0-85.0)
Interstitial Fibrosis/ Tubular Atrophy (IFTA)	
IFTA = 0	8
IFTA = 2	4
IFTA = 4	2
IFTA = 6	5
Categories	
eGFR > 45 & IFTA = 0	4
eGFR > 45 & IFTA > 0	3
eGFR ≤ 45 & IFTA = 0	4
eGFR ≤ 45 & IFTA > 0	8

Site 1 patients were recruited from kidney transplant recipients with either acute or chronic allograft injury undergoing percutaneous clinically indicated biopsies, while Site 2 patients recruited kidney transplant recipients undergoing percutaneous clinically indicated biopsies and patients undergoing surveillance biopsy in the setting of donor specific antibody positivity. The decision to perform percutaneous allograft biopsy was based on the clinician's adjudication of each patient's clinical presentation regarding institute specific management or prognostication. Mean age and gender distribution ($\chi^2 = 1.25, p = 0.263$) were not significantly different between the two sites though Site 2 recruited patients with a statistically higher average BMI. As Site 1 and Site 2 recruited different subsets of kidney transplant recipients, in line with expectations Site 2 had a greater number of low IFTA scored patients, and a higher average eGFR due to the surveillance biopsies.

Supplement B. Supplementary Tables: Fibrosis Scores

Tabular Data of Spectral Diffusion, IVIM, and ADC values between (a) no fibrosis (IFTA=0) vs. fibrosis (IFTA >0), (b) no fibrosis vs. mild/moderate fibrosis (IFTA=1-4), and (c) no fibrosis vs. severe fibrosis (IFTA=5-6). Features that returned a raw $p < 0.05$ are colored red. Features that passed the Benjamini-Hochberg correction with $fpr = 0.20$ are highlighted yellow.

Supplement C. Supplementary Tables: AllograftGroups

Tabular Data of Spectral Diffusion, IVIM, and ADC values between allografts with normal/stable function ($\text{eGFR} \geq 45 \text{ ml/min/1.73m}^2$) and no fibrosis ($\text{IFTA} = 0$) versus (a) normal/stable function and fibrosis ($\text{IFTA} > 0$), (b) impaired function and no fibrosis, and (c) impaired function ($\text{eGFR} < 45 \text{ ml/min/1.73m}^2$) and fibrosis. Features that returned a raw $p < 0.05$ are colored red. Features that passed the Benjamini-Hochberg correction with $\text{fpr} = 0.20$ are highlighted yellow

Supplement D. Supplementary Tables: Interobserver Repeatability

Tabular Data of interclass correlation coefficient and corresponding F-stat and 95% CI for all parameters. The coefficient of variability is also provided. There is a low ICC for median fD tubule (ICC=0.03), due to low agreement of median f tubule ICC (0.04), as many f tubules are zero.

Interobserver Repeatability				
Feature	ICC value	F-stat	95% CI	CoV% value
spectral mean f vascular	0.75	7.1	[0.46 0.9]	25.914
spectral median f vascular	0.78	8.29	[0.52 0.91]	62.053
spectral std f vascular	0.44	2.57	[-0. 0.74]	22.751
spectral mean f tubule	0.35	2.1	[-0.11 0.69]	40.850
spectral median f tubule	0.04	1.09	[-0.41 0.48]	75.356
spectral std f tubule	0.55	3.42	[0.14 0.8]	30.253
spectral mean f tissue	0.47	2.78	[0.03 0.76]	5.148
spectral median f tissue	0.35	2.06	[-0.12 0.68]	4.457
spectral std f tissue	0.54	3.38	[0.13 0.8]	16.285
spectral mean D vascular	0.64	4.53	[0.27 0.84]	18.854
spectral median D vascular	0.38	2.22	[-0.08 0.7]	56.568
spectral std D vascular	0.11	1.24	[-0.35 0.53]	7.396
spectral mean D tubule	0.58	3.81	[0.19 0.82]	23.631
spectral median D tubule	0.4	2.34	[-0.05 0.72]	65.052
spectral std D tubule	0.76	7.3	[0.48 0.9]	18.990
spectral mean D tissue	0.21	1.55	[-0.25 0.6]	7.001
spectral median D tissue	0.45	2.65	[0.01 0.75]	5.724
spectral std D tissue	0.3	1.87	[-0.16 0.66]	15.868
spectral mean fD vascular	0.42	2.46	[-0.03 0.73]	9.325
spectral mean fD tubule	0.25	1.68	[-0.21 0.63]	50.211
spectral mean fD tissue	0.71	5.95	[0.39 0.88]	65.881
spectral median fD vascular	0.4	2.32	[-0.06 0.72]	10.330
spectral median fD tubule	0.03	1.06	[-0.42 0.47]	79.441
spectral median fD tissue	0.79	8.64	[0.54 0.91]	34.441
IVIM mean D	0.76	7.39	[0.48 0.9]	2.237
IVIM median D	0.67	5.12	[0.33 0.86]	2.421
IVIM std D	0.89	16.89	[0.73 0.96]	6.088
IVIM mean D*	0.81	9.48	[0.57 0.92]	11.101
IVIM median D*	0.55	3.43	[0.14 0.8]	10.649
IVIM std D*	0.92	23.97	[0.8 0.97]	15.268
IVIM mean f	0.66	4.82	[0.3 0.85]	5.694
IVIM median f	0.63	4.38	[0.26 0.84]	5.517
IVIM std f	0.32	1.92	[-0.15 0.67]	14.865
IVIM mean (1-f)D	0.78	8.2	[0.52 0.91]	3.114
IVIM median (1-f)D	0.71	6.01	[0.4 0.88]	3.140
IVIM mean fD*	0.73	6.52	[0.43 0.89]	13.477
IVIM median fD*	0.56	3.58	[0.16 0.81]	11.270
mean ADC	0.84	11.3	[0.63 0.93]	2.868
median ADC	0.79	8.74	[0.54 0.92]	3.069
std ADC	0.62	4.26	[0.24 0.83]	11.220

Supplement E. Spectral Diffusion and Multi-Component Diffusion fD

Spectral peaks were sorted into (1) vascular, (2) tubular, and (3) tissue parenchyma components based on diffusion coefficient. A spectrum with peaks in each of the three components listed above would be a tri-exponential, as follows.

$$f_{\text{vasc}}e^{-bD_{\text{vasc}}} + f_{\text{tubule}}e^{-bD_{\text{tubule}}} + f_{\text{tissue}}e^{-bD_{\text{tissue}}}$$

In this work, these three components are ordered from left to right from fastest to slowest diffusion coefficient. The peaks were sorted as follows: the largest peak closest to $1.8 \times 10^{-3} \text{ mm}^2/\text{s}$, a tissue diffusion literature value between two-component and three-component rigid fits⁸, was considered the tissue parenchyma peak if below $50 \times 10^{-3} \text{ mm}^2/\text{s}$. Beyond that, peaks were sorted as $0.8 \leq \text{tissue} < 5 \leq \text{tubule} < 50 \leq \text{vascular}$ for diffusion coefficients in units of $10^{-3} \text{ mm}^2/\text{s}$. The boundary of $5 \times 10^{-3} \text{ mm}^2/\text{s}$ for tissue parenchyma is higher than $2 \times 10^{-3} \text{ mm}^2/\text{s}$ to include the boundary of the edge of the tissue peak, even though the peak's maximum is closer to $2 \times 10^{-3} \text{ mm}^2/\text{s}$ (Figure 1). If more than one peak fell within a certain range, the peaks were combined weighted by their respective volume fractions for statistical analysis of diagnostic ability. Peaks with mean $D < 0.8$ were excluded due to $b=800$ being too low to capture very slow diffusion reliably¹¹.

fD of each peak was treated as a multi-component flow proxy as described in Liu et al¹³. With a Gaussian approximation of each physiologic component⁴⁸, fD was used to estimate the amount of flow of any distinct diffusion component, without capillary network assumptions of conventional IVIM perfusion. Further, as the signal labeling and readout are in the same plane^{51,52}, fD calculates local flow without needing an AIF⁵³⁻⁵⁶. Therefore, fD may provide information on local tissue diffusion, tubular flow, and perfusion without the complexities of selecting an aortic AIF⁵⁷, a labeling-plane for ASL, or correction for delayed and dispersed contrast a local-AIF⁵⁸. Further, non-vascular flow that may not have an AIF, such as diffusion in the renal tubules, can still be imaged with spectral diffusion.

Supplement F. Clinical notes

Table A1. Further clinical notes and diagnoses for the 14 patients with allografts that showed impaired function but no fibrosis in this preliminary study.

Patient 1	Active antibody mediated rejection, Chronic active antibody mediated rejection, Chronic active T-cell mediated rejection Grade II, Suspicious or borderline for acute T-cell mediated rejection, Transplant glomerulopathy, moderate glomerulitis, multilayering of interstitial capillary basement membranes, and focally positive (2+) C4d staining of interstitial capillaries, Arteriolar hyalinosis. protein droplets in podocytes positive for albumin and kappa
Patient 2	Active antibody mediated rejection, Acute/active T-cell mediated rejection Grade IB, Acute/active T-cell mediated rejection Grade III, Acute/active vascular rejection Grade III, Recurrent disease, Focal segmental glomerulosclerosis, NOS.
Patient 3	C4d deposition without evidence of rejection, Acute tubular injury, Focal crystals consistent with calcium phosphate, Mild arteriosclerosis. There is no significant tubular or interstitial staining for IgG, IgA, IgM, C3, C1q, Kappa and Lambda light chains, albumin, and fibrinogen.
Patient 4	Acute tubular injury, Thin glomerular basement membranes
Patient 5	Acute tubular injury. There is no significant glomerular, tubular, or interstitial staining for IgG, IgA, IgM, C3, C1q, Kappa and Lambda light chains, albumin, and fibrinogen.
Patient 6	Mild glomerulitis, Mild interstitial lymphoid infiltrates. a scarred region of the glomerulus shows nonspecific smudgy staining for IgM, C3 and C1q
Patient 7	None
Patient 8	1+ C3 seen in vessels, Polyomavirus Nephritis (01_64)
Patient 9	Mild acute tubular injury
Patient 10	negative CD4
Patient 11	None
Patient 12	Mild glomerulitis
Patient 13	None
Patient 14	Mild glomerulitis